

Gallium doped n-type $Zn_xCd_{1-x}S$ nanoribbons: Synthesis and photoconductivity properties

Li Wang, Xiang-An Wang, Ran Chen, Chun-Yan Wu, Yong-Qiang Yu, Jun Xu, Ji-Gang Hu, and Lin-Bao Luo

Citation: *Journal of Applied Physics* **115**, 063108 (2014); doi: 10.1063/1.4865740

View online: <http://dx.doi.org/10.1063/1.4865740>

View Table of Contents: <http://scitation.aip.org/content/aip/journal/jap/115/6?ver=pdfcov>

Published by the AIP Publishing

Articles you may be interested in

[p-type ZnS:N nanowires: Low-temperature solvothermal doping and optoelectronic properties](#)

Appl. Phys. Lett. **103**, 213111 (2013); 10.1063/1.4833275

[Magnetic behaviour of Fe-doped CdS diluted magnetic semiconducting nanocrystalline thin films](#)

J. Appl. Phys. **112**, 043907 (2012); 10.1063/1.4748270

[Synthesis and characterization of Mn doped ZnS nanometer-sized particles](#)

AIP Conf. Proc. **1447**, 217 (2012); 10.1063/1.4709957

[ZnO homojunction photodiodes based on Sb-doped p-type nanowire array and n-type film for ultraviolet detection](#)

Appl. Phys. Lett. **98**, 041107 (2011); 10.1063/1.3551628

[Study of composition dependent structural, optical, and magnetic properties of Cu-doped \$Zn_{1-x}Cd_xS\$ nanoparticles](#)

J. Appl. Phys. **108**, 123519 (2010); 10.1063/1.3524516

The logo for AIP APL Photonics is displayed. It features the letters 'AIP' in a large, white, sans-serif font on the left, followed by a vertical line and the words 'APL Photonics' in a smaller, white, sans-serif font on the right. The background is a vibrant red with a bright yellow sunburst effect emanating from the top right corner.

APL Photonics is pleased to announce
Benjamin Eggleton as its Editor-in-Chief



Gallium doped n -type $\text{Zn}_x\text{Cd}_{1-x}\text{S}$ nanoribbons: Synthesis and photoconductivity properties

Li Wang,^{1,2,a)} Xiang-An Wang,¹ Ran Chen,¹ Chun-Yan Wu,¹ Yong-Qiang Yu,¹ Jun Xu,¹ Ji-Gang Hu,¹ and Lin-Bao Luo^{1,a)}

¹*School of Electronic Science and Applied Physics and Anhui Provincial Key Laboratory of Advanced Materials and Devices, Hefei University of Technology, Hefei, Anhui 230009, People's Republic of China*

²*Department of Materials Science and Engineering, University of Toronto, Toronto, Ontario M5S 3E4, Canada*

(Received 28 November 2013; accepted 29 January 2014; published online 13 February 2014)

Gallium doped $\text{Zn}_x\text{Cd}_{1-x}\text{S}$ nanoribbons (NRs) with controlled composition were synthesized on Au-coated Si (100) substrates by a simple thermal co-evaporation method. The composition of $\text{Zn}_x\text{Cd}_{1-x}\text{S}:\text{Ga}$ NRs can be simply controlled by the distance of the substrates from the source powder. The grown NRs exhibit excellent crystallinity, with growth direction along [0002]. It is found that the gallium doping can remarkably enhance the conductivity of $\text{Zn}_x\text{Cd}_{1-x}\text{S}:\text{Ga}$ NRs, leading to obvious n -type conduction behavior. It is also observed that the $\text{Zn}_x\text{Cd}_{1-x}\text{S}:\text{Ga}$ NRs show sensitive photoresponse to visible light illumination with excellent stability and reproducibility. The generality of this study suggests the great potential of the $\text{Zn}_x\text{Cd}_{1-x}\text{S}:\text{Ga}$ NRs for future optoelectronics application. © 2014 AIP Publishing LLC. [<http://dx.doi.org/10.1063/1.4865740>]

INTRODUCTION

The direct band-gap sulfides of group II-VI, such as ZnS and CdS, are attractive candidates for the developing high-performance optical and optoelectronic devices.¹ ZnS (Eg \approx 3.7 eV), one of the semiconductors discovered earliest, plays a very important role in the electric and optoelectronic industries, especially for short wavelength light emitting diodes (LEDs) and heterojunction devices.^{2,3} CdS, with a narrow band-gap of 2.42 eV and an exciton binding energy of 28 meV, has been widely used to fabricate optically and electrically driven laser emission devices, solar cells,⁴ photocatalytic materials, and optical sensors.⁵ More recently, ternary semiconductor compound have been receiving increasing research interest for their excellent optical properties and easy synthesis. Continuous series of $\text{Zn}_x\text{Cd}_{1-x}\text{S}$ solid solutions, for example, can be formed with CdS and ZnS by the Cd and Zn atoms substitute to each other in the crystal lattice. The functional properties of $\text{Zn}_x\text{Cd}_{1-x}\text{S}$ can be readily tailored by varying the stoichiometric ratio of the system ($0 \leq x \leq 1$), which makes $\text{Zn}_x\text{Cd}_{1-x}\text{S}$ more attractive and widely used in devices application.⁶ It has been reported that combining metal sulfides with other semiconductors or doping metal sulfides with transition metal elements can greatly improve their photocatalytic activity and stability.⁷

For all semiconductor materials, band gap energy is a very important parameter determining their electronic and optical properties. The band gap of $\text{Zn}_x\text{Cd}_{1-x}\text{S}$ can be tailored in a wide range from 2.4 to 3.7 eV, corresponding to visible to UV spectral range. By this token, $\text{Zn}_x\text{Cd}_{1-x}\text{S}$ can be employed to fabricate LED sources with controlled multicolor emission or photodetectors responding in a large range.⁶ $\text{Zn}_x\text{Cd}_{1-x}\text{S}$ can also replace CdS as the window layer to avoid absorption of the blue portion of the solar spectrum,⁷ or ZnS as

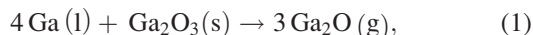
photocatalysts with smaller band gaps to harvest visible light.⁸ This kind of composition-dependent band gap is more stable than small scale size-dependent band gap due to the size disparities.^{9–11} Nevertheless, it is undeniable that the high quality single-crystal $\text{Zn}_x\text{Cd}_{1-x}\text{S}$ films or bulks are difficult to synthesize due to low crystallinity of II-VI Zn based ternary,¹² which hampers their potential application in various optoelectronics. The advance of the nanofabrication provides a solution to overcome this problem. High-quality single-crystal group II-VI nanomaterials with fewer defects can be synthesized on large scale by a co-thermal evaporation method.⁹ To date, while great progresses have been made in the fabrication,^{7,8,10} microstructure,^{13–15} and optical properties of $\text{Zn}_x\text{Cd}_{1-x}\text{S}$ nanostructures,^{16–19} studies on the doping and electrical transport properties of ternary $\text{Zn}_x\text{Cd}_{1-x}\text{S}$ nanostructures are rare. Exploration along this direction is highly desirable considering the fact that doping is vitally important for further optoelectric devices application. Herein, we describe the synthesis of $\text{Zn}_x\text{Cd}_{1-x}\text{S}$ nanoribbons (NRs) with tunable compositions of $X = 0.05, 0.1, 0.21, 0.92, 0.95$, which was doped by gallium by using a mixed powder of Ga and Ga_2O_3 through a thermal co-evaporation method. Electrical analysis of the Ga doped $\text{Zn}_x\text{Cd}_{1-x}\text{S}$ NR reveals that the conductivity of the $\text{Zn}_x\text{Cd}_{1-x}\text{S}$ NRs was remarkably enhanced upon doping. In addition, the NRs exhibit obvious n -type conduction behavior. The time response spectra of the NR photodetector to pulsed light show excellent stability and reproducibility. This study suggests the great potential of the Ga-doped $\text{Zn}_x\text{Cd}_{1-x}\text{S}$ NRs for future nano-optoelectronics devices application.

EXPERIMENTAL DETAILS

The synthesis of the Ga-doped $\text{Zn}_x\text{Cd}_{1-x}\text{S}$ NRs was carried out on a horizontal tube furnace using ZnS (Aldrich, 99.99%) and CdS (Aldrich, 99.99%) as the source material via a simple co-thermal evaporation method. A mixed powder of Ga and Ga_2O_3 was introduced into the system as the

^{a)}Author to whom correspondence should be addressed. Electronic addresses: wlhgd@hfut.edu.cn and luolb@hfut.edu.cn.

dopants instead of Ga for the high boiling points of metal Ga ($\sim 2400^\circ\text{C}$). The molar ratio of Ga:Ga₂O₃ is set to be 4:1, which will favor the generation of Ga vapor *via* the following chemical reactions:²⁰



In a typical experiment, ZnS powder (0.1 g) was first loaded into an alumina boat and then transferred to the center position of the furnace. Another boat filled with a 0.1 g mixed powder of CdS, Ga, and Ga₂O₃ (the content of Ga and Ga₂O₃ was 10%) was placed near the ZnS source in the upstream direction. To control the composition of the product by deposition temperature, silicon substrate coated with 10 nm Au catalysts was placed vertically at the downstream, around 10, 10.5, 11, 11.5 and 12 cm away from the ZnS source (as shown in Scheme 1) each time. The reaction chamber was filled with a gas mixture of 30 standard-state cubic centimeter per minute (sccm) Ar and H₂ (5% in volume) after it was evacuated to a base pressure of 10^{-5} Torr. The pressure in the tube was adjusted to 180 Torr before heating. Then the temperatures of ZnS powder was increased to 1050°C and maintained for about 2 h. When the system was cooled down to room temperature, the Si substrates were taken out of the furnace. Lays of wool-like products could be observed on the substrate. In this work, five kinds of samples were synthesized, and marked as S₁, S₂, S₃, S₄, and S₅ according to the decreasing distances between Si substrate and ZnS source.

The structures and morphologies of the as-synthesized products were characterized by X-ray diffraction (XRD, Rigaku D/Max-g B, with Cu-K α radiation), field-emission scanning electron microscopy (FESEM, Philips XL 30 FEG), and high-resolution transmission electron microscopy (HRTEM, JEOL-2010). The chemical compositions of the products were analyzed by energy-dispersive X-ray spectroscopy (EDX, attached to the SEM) and X-ray photoelectron spectroscopy (XPS, VGESCALAB MKII). Room-temperature photoluminescence (PL) spectra were measured using a 325 nm He-Cd laser as the excitation source (LABRAM-HR). To evaluate the electrical and photoconductive properties of the Ga-doped Zn_xCd_{1-x}S NRs, nano-metal-oxide-semiconductor FETs (nano-MOSFET) were constructed based on individual NRs. Briefly, the as-doped Zn_xCd_{1-x}S NRs were first dispersed on a SiO₂ (300 nm)/p⁺-Si substrate, and subsequently photolithography and lift-off processes were used to define the source and drain electrodes on the NRs. The degenerately doped Si substrate acted as the global back gate. All the electrical measurements were conducted at room temperature

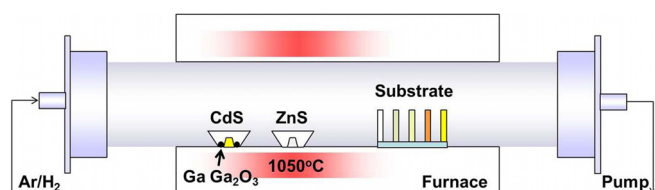


FIG. 1. Schematic illustration of the setup for the synthesis of Zn_xCd_{1-x}S nanoribbons.

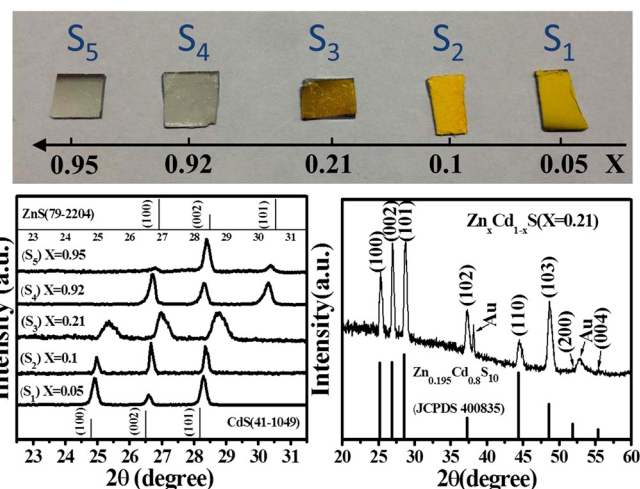


FIG. 2. (a) Digital camera pictures of all the five samples; (b) XRD patterns of gallium doped Zn_xCd_{1-x}S nanoribbons synthesized with different distances between Si substrate and ZnS source: S₁, S₂, S₃, S₄, and S₅; (c) XRD pattern of S₃ and the JCPDS card No. 40-0835.

with a semiconductor character system (Keithley 4200-SCS). To analyze the photoconductive properties of Zn_xCd_{1-x}S NRs, white light from the optical microscopy on the probe station and a monochromatic light from a source composed of a xenon lamp (500 W) through a monochromator (Omni- λ 300) were introduced into the test system.

RESULT AND DISCUSSION

The fabrication of the NRs was carried out on a CVD furnace as shown in Figure 1. Figure 2(a) displays the as-collected undoped Zn_xCd_{1-x}S samples, according to which the color changes gradually from yellow to silver with the increase of X. To study the phase and crystallinity of these samples, all the Zn_xCd_{1-x}S samples were characterized by XRD in the

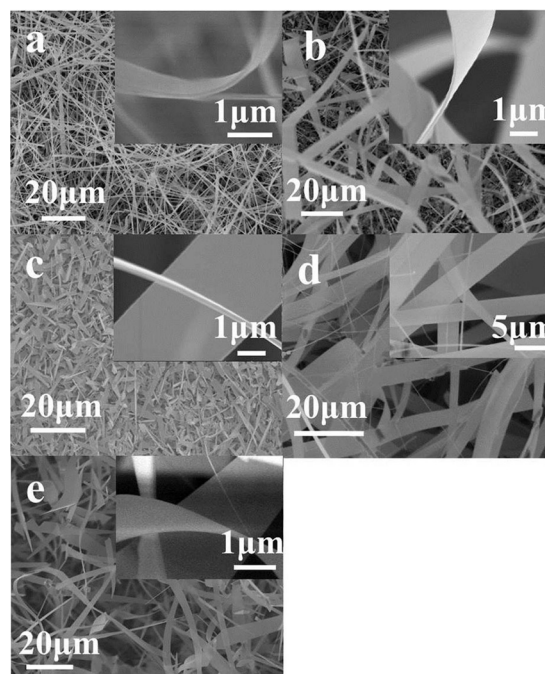


FIG. 3. Representative scanning electron microscopy images of the gallium doped Zn_xCd_{1-x}S NRs: S₅ (a), S₄ (b), S₃ (c), S₂ (d), S₁ (e).

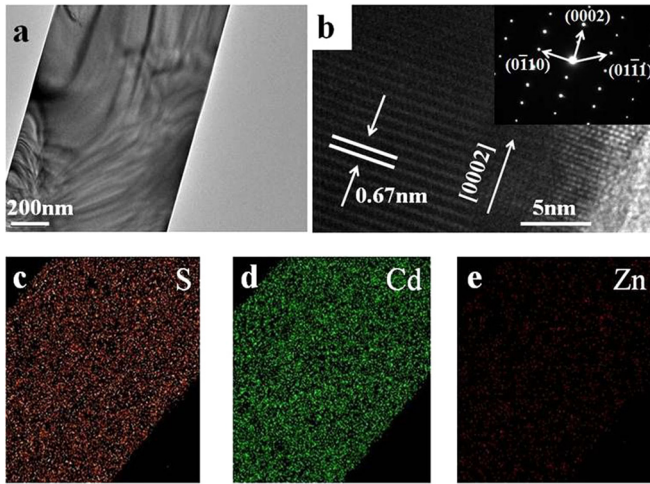


FIG. 4. (a) Typical TEM bright-field image of an individual $Zn_xCd_{1-x}S$ NR (S_1), (b) corresponding HRTEM image, and the inset is the SAED image. (c-e) elemental mapping images for S (c), Cd (d), and Zn (e), respectively.

range of $22\text{--}32^\circ$, for comparison, the JCPDS (Joint Committee on Powder Diffraction Standards) cards No. 79-2204 (ZnS) and No. 41-1049 (CdS) marked with solid lines was provided as well (Figure 2(b)). It is found that all the products can be readily indexed to hexagonal phase. The diffraction peaks for the (100) plane are located at 24.9 , 25 , 25.3 , 26.7 , and 26.8° , respectively. For such a ternary $Zn_xCd_{1-x}S$ nanostructure, the lattice parameters of the NR have a linear dependence on the constant X. This relationship, known as Vegard's law, can be described by the formula of $C_x = C_{CdS} + (C_{ZnS} - C_{CdS})x$, where C_{ZnS} , C_{CdS} and C_x are the c -axis lattice constants of the hexagonal structures of ZnS , CdS , and $Zn_xCd_{1-x}S$, respectively.^{21,22} Based on this formula and Bragg reflection equation, we selected the diffraction angles corresponding to the (100) and (002) planes and calculated the constant X for all five samples (see Figure 2(b)). It is worth noting that the XRD data of

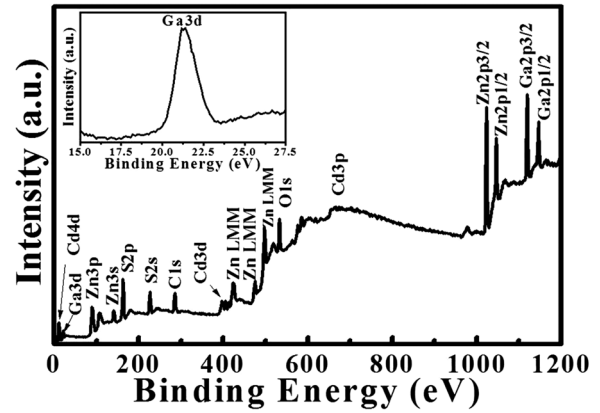


FIG. 5. XPS analysis of the Ga doped $Zn_{0.95}Cd_{0.05}S$ (S_5) nanoribbons.

sample S_3 ($Zn_{0.21}Cd_{0.79}S:Ga$ NRs) match well with the JCPDS card No. 40-0835 of $Zn_{0.195}Cd_{0.8}S$, which suggests that our calculation of constant X is reliable with the consideration of composition fluctuation (0.02) within the XRD probe size (see Figure 2(c)).

The as-synthesized samples were then transferred into SEM chamber for morphology characterization. As shown in Figure 3, all the samples are composed of long ribbon-like nanostructures. The surfaces of $Zn_xCd_{1-x}S$ NRs are clean and smooth without visible particles and impurities. Specifically, the $Zn_xCd_{1-x}S$ NRs have typical width in the range of $1\ \mu\text{m}\text{--}5\ \mu\text{m}$ and thickness of $20\text{--}90\ \text{nm}$. What is more, there is obvious variation in width and thickness of different samples, which should be related to the growth temperature and composition. The length of all the $Zn_xCd_{1-x}S$ NRs is about hundreds of micrometers, which is highly favorable for subsequent nanodevice fabrication.

To further study the microstructure of the as-prepared gallium doped $Zn_xCd_{1-x}S$ NRs, we characterize both TEM and high-resolution TEM analysis. Figure 4 shows a typical

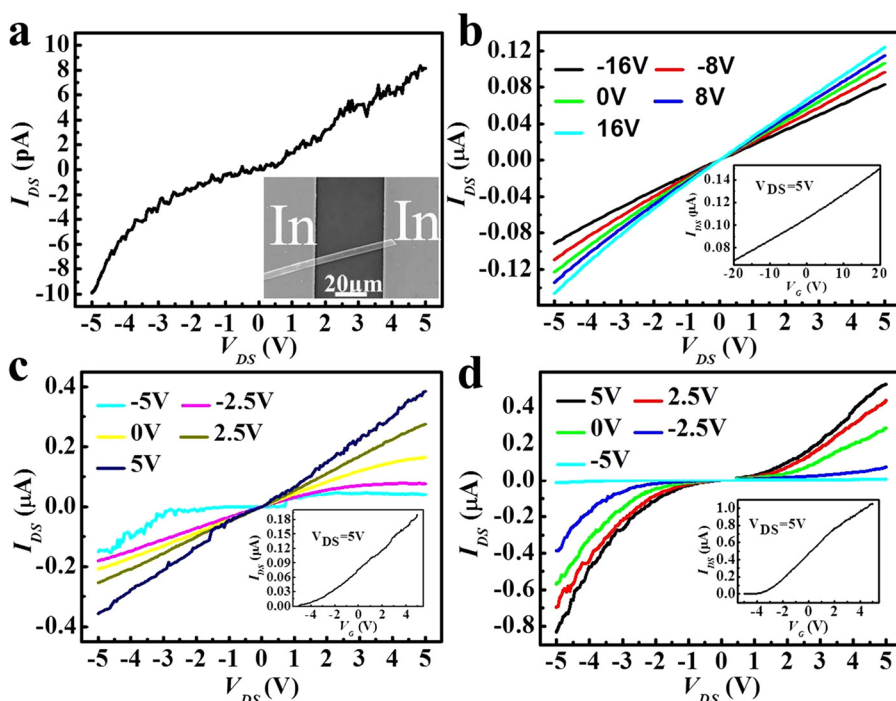


FIG. 6. (a) I - V curves of the undoped $Zn_xCd_{1-x}S$ NR, the inset shows the SEM image of the nanodevice; (b) I_{DS} - V_{DS} curves of S_5 ($Zn_{0.95}Cd_{0.05}S$) measured at varied V_G , the V_G increases from -16 to $16\ \text{V}$ at a step of $8\ \text{V}$, the inset shows the I_{DS} - V_G curve at $V_{DS} = 5\ \text{V}$; (c-d) I_{DS} - V_{DS} curves of S_3 ($Zn_{0.21}Cd_{0.79}S$) and S_1 ($Zn_{0.05}Cd_{0.95}S$) measured at varied V_G , the V_G increases from -5 to $5\ \text{V}$ at a step of $2.5\ \text{V}$, the inset shows the I_{DS} - V_G curve at $V_{DS} = 5\ \text{V}$ with a step of $2.5\ \text{V}$.

TABLE I. Summary of the key device parameters of the NR-based FETs.

Sample	σ (S·cm ⁻¹)	g_m (nS)	n ($\times 10^{17}$ cm ⁻³)	μ_n (cm ² ·V ⁻¹ ·s ⁻¹)
S ₁ Zn _{0.05} Cd _{0.95} S:Ga	0.26	111.99	1.24	13.5
S ₃ Zn _{0.21} Cd _{0.79} S:Ga	0.08	26.96	1.98	2.81
S ₅ Zn _{0.95} Cd _{0.05} S:Ga	0.29	2.02	25.8	0.69

TEM image of S₁ (Zn_{0.05}Cd_{0.95}S), from which one can see that the NR has a well-defined single-crystal hexagonal structure. The HRTEM image of the S₁ in Figure 4(b) shows a d -spacing of 0.67 nm, corresponding to the lattice spacing of (0002) plane, suggesting that the preferential growth direction of the NR is along [0002]. The elemental maps displayed in Figures 4(c)–4(e) shows the uniformly distribution of the constituting elements, that is Zn, Cd, and S. Note that the mapping profile of gallium atom was not shown here in that its concentration is below the resolution. Figure 5 shows the corresponding X-ray photoelectron spectroscopy (XPS) of S₅. It is found that in addition to the signal of Zn, Cd, and S atoms, a weak peak at 1118 eV with content of 1.45 at. %, due to the Ga_{2p_{3/2}} core level appeared, implying that Ga atoms is successfully incorporated into the Zn_xCd_{1-x}S NRs.

To evaluate the effect of Ga doping on the transport properties of the NRs, field-effect transistors (FETs) were constructed based on individual NR. Figure 6(a) shows typical I - V curves of the undoped Zn_xCd_{1-x}S NR (the SEM image of the device is shown in the inset). Obviously, the Zn_xCd_{1-x}S NR without Ga doping are highly insulative with a conductivity as low as $\sim 8.2 \times 10^{-8}$ S cm⁻¹. In contrast, the NR conductivity can be dramatically improved by 7 orders of magnitude, to 0.29, 0.08, and 0.26 S cm⁻¹ corresponding to S₅ (Zn_{0.95}Cd_{0.05}S), S₃ (Zn_{0.21}Cd_{0.79}S), and S₁ (Zn_{0.05}Cd_{0.95}S) NRs (Figures 6(b)–6(d)). According to the source drain current (I_{DS}) versus source drain voltage (V_{DS}) curves (Figures 6(b)–6(d)) measured at varied V_G , the FETs device exhibits

pronounced gating effects. The insets of Figures 6(b)–6(d) show the transfer characteristics (I_{DS} - V_{GS}) of the device, from which, one can see that I_{DS} increases monotonously with increasing V_{GS} , in consistence with the typical behavior of an n -channel FET. Table I summarizes the key parameters of the nano-FETs that are fabricated from the Zn_xCd_{1-x}S NR with varied compositions, in which the electron mobility (μ_n) can be estimated from the channel transconductance (g_m) of the nano-FETs, by using equation $g_m = dI_{DS}/dV_{GS} = Z\mu_n C_0 V_{DS}/L$ in the linear regime of I_{DS} - V_G curves [insets in Figures 6(b)–6(d)], where Z/L is the width-to-length ratio of the NR channel, and C_0 is the oxide capacitance per unit area.²³ The electron concentration (n) can be calculated from the equation $n = \sigma/q\mu_n$, where σ is the conductivity of the NRs at $V_{GS} = 0$ V. From Table I, it is found that n increases remarkably with the increase of Zn content and achieve the highest electron concentration of 2.58×10^{18} cm⁻³ for S₅. In contrast, the μ_n is observed to decrease with the increasing Zn content, which might be due to enhanced carrier scattering, and low μ_n of ZnS compared with CdS.

Figures 7(a)–7(c) show the time response spectra of a single Zn_xCd_{1-x}S NR measured under pulsed white light at an external bias voltage of 5 V. Apparently, all the three devices can be easily switched between high- and low-conduction states when the light was turned on and off alternatively. The rising and decaying photocurrent follows an exponential function, which can be fit with the equations²⁴

$$I(t) = I_0 + A_1(1 - e^{-\frac{t}{\tau_{r1}}}) + A_2(1 - e^{-\frac{t}{\tau_{d2}}}), \quad (3)$$

$$I(t) = I_0 + A_3e^{-\frac{t}{\tau_{d1}}} + A_4e^{-\frac{t}{\tau_{d2}}}, \quad (4)$$

where I_0 is the dark current, A_1 , A_2 , A_3 , and A_4 are positive constants. τ_{r1} , τ_{r2} and τ_{d1} , τ_{d2} are time constants for rising and decaying photocurrent, respectively. The calculated parameters of the time response spectra are summarized in

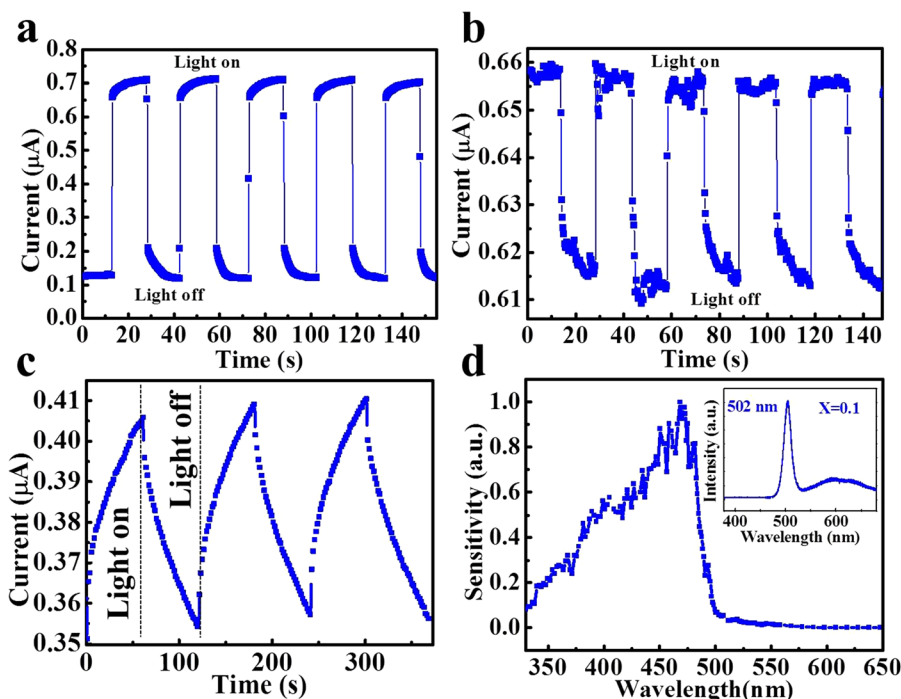


FIG. 7. (a-c) Time response spectra of the devices made from (a) S₁ (Zn_{0.05}Cd_{0.95}S), (b) S₃ (Zn_{0.21}Cd_{0.79}S), and (c) S₅ (Zn_{0.95}Cd_{0.05}S) at 5 V under pulsed light illumination, The white light was turned on/off manually to generate the pulsed light; (d) Spectral response of the S₁ (Zn_{0.05}Cd_{0.95}S) NR measured at a constant light intensity of $\sim 72 \mu\text{Wcm}^{-2}$ at $V_{DS} = +5$ V, and the insert is the room temperature PL spectrum of S₁ (Zn_{0.05}Cd_{0.95}S).

TABLE II. Summary of the photoconductive properties of the ZnCdS:Ga NRs.

Sample	I_{on}/I_{off}	τ_{r1} (s)	τ_{r2} (s)	τ_{d1} (s)	τ_{d2} (s)
S ₁ Zn _{0.05} Cd _{0.95} S:Ga	5.6	0.37	0.11	0.38	0.85
S ₃ Zn _{0.21} Cd _{0.79} S:Ga	1.1	0.64	0.32	1.27	2.54
S ₅ Zn _{0.95} Cd _{0.05} S:Ga	1.2	12	48	1.4	58

Table II, according to which, the time constants from fitting for S₁ are $\tau_{r1} = 0.37$ s, $\tau_{r2} = 0.11$ s, $\tau_{d1} = 0.38$ s, $\tau_{d2} = 0.85$ s. Similar fittings were performed for S₃ and resulted in rise time of $\tau_{r1} = 0.64$ s, $\tau_{r2} = 0.32$ s and decay time constants of $\tau_{d1} = 1.27$ s and $\tau_{d2} = 2.54$ s. By comparison, the time constants for the S₅ are much larger than S₁ and S₃, $\tau_{r1} = 12$ s, $\tau_{r2} = 48$ s, $\tau_{d1} = 1.4$ s, $\tau_{d2} = 58$ s. The relatively slow response speed for S₅ can be ascribed to the huge amount of trapping centers as a result of higher doping level.²⁵ At last, the spectral selectivity of device was studied. Figure 7(d) shows the typical photoresponse of S₁ NR when exposed to the monochromatic light with varied wavelength (λ) at a constant light intensity of $\sim 72 \mu\text{Wcm}^{-2}$. It is seen that the conductance of the S₁ NR is very low upon the 350 nm light illumination, but it gradually increases with the decrease of the light wavelength and reaches the maximum at 470 nm. However, when the wavelength continues to increase, the conductance of the NR begins to decrease. The sensitivity of the NR photodetector is rather low (<2%) for the wavelength longer than 500 nm. The cut-off wavelength of the device is estimated to be 500 nm, corresponding to the band-gap emission of S₁ (Zn_{0.05}Cd_{0.95}S) of 2.47 eV derived from the emission band (insert of Figure 6(d)). As matter of factor, similar phenomenon has been previously observed in CdS NRs (Ref. 26) and SnO₂ nanowires.²⁷ We believe this agreement is highly related to the photoconductive mechanism. Namely, the photoresponse of the NR to light illumination is a process of carrier generation. Under light irradiation, only photons with sufficient energy can lift electrons from the valance band to conduction band. Photons with insufficient energy cannot excite electrons and therefore cannot contribute to the photoresponse.

CONCLUSION

In summary, Ga doped Zn_xCd_{1-x}S NRs with tunable compositions of $x = 0.05, 0.1, 0.21, 0.92, 0.95$, were fabricated by a simple thermal evaporation method. The electrical conductivity of Zn_xCd_{1-x}S NRs was substantially improved compared with the undoped ones. It is also observed that the Zn_xCd_{1-x}S NRs exhibit stable and reproducible photoresponse to white light illumination, with excellent spectral selectivity. The totality of this study suggests the great

potential of these Ga doped Zn_xCd_{1-x}S NRs for future high-performance optoelectronic devices application.

ACKNOWLEDGMENTS

This work was supported by the financial supports from the China Scholarship Council, Natural Science Foundation of China (Nos. 61106010, 21101051, 21301044), and the Fundamental Research Funds for the Central Universities (Nos. 2013HGXJ0195, 2012HGCX0003, 2013HGCH0012).

- ¹J. S. Jie, W. J. Zhang, I. Bello, C. S. Lee, and S. T. Lee, *Nano Today* **5**, 313 (2010).
- ²J. A. Zapien, Y. Jiang, X. M. Meng, W. Chen, F. C. K. Au, Y. Lifshitz, and S. T. Lee, *Appl. Phys. Lett.* **84**, 1189 (2004).
- ³Y. Jiang, W. J. Zhang, J. S. Jie, X. M. Meng, and J. A. Zapien, S. T. Lee, *Adv. Mater.* **18**, 1527 (2006).
- ⁴F. Z. Li, L. B. Luo, Q. D. Yang, D. Wu, C. Xie, B. Nie, J. S. Jie, C. Y. Wu, L. Wang, and S. H. Yu, *Adv. Energy. Mater.* **3**, 579 (2013).
- ⁵S. K. Apte, S. N. Garaje, G. P. Mane, A. Vinu, S. D. Naik, D. P. Amalnerkar, and B. B. Kale, *Small* **7**, 957 (2011).
- ⁶T. Y. Lui, J. A. Zapien, H. Tang, D. D. Ma, Y. K. Liu, C. S. Lee, S. T. Lee, S. L. Shi, and S. J. Xu, *Nanotechnology* **17**, 5935 (2006).
- ⁷W. J. Li, D. Z. Li, W. J. Zhang, Y. Hu, Y. H. He, and X. Z. Fu, *J. Phys. Chem. C* **114**, 2154 (2010).
- ⁸S. L. Xie, X. H. Lu, T. Zhai, J. Y. Gan, W. Li, M. Xu, M. H. Yu, Y. M. Zhang, and Y. X. Tong, *Langmuir* **28**, 10558 (2012).
- ⁹Y. K. Liu, J. A. Zapien, Y. Y. Shan, C. Y. Geng, C. S. Lee, and S. T. Lee, *Adv. Mater.* **17**, 1372 (2005).
- ¹⁰L. Z. Wang, Y. Jiang, C. Wang, W. H. Wang, B. L. Cao, M. Niu, and Y. T. Qian, *J. Alloys Compd.* **454**, 255 (2008).
- ¹¹A. L. Pan, H. Yang, R. B. Liu, R. C. Yu, B. S. Zou, and Z. L. Wang, *J. Am. Chem. Soc.* **127**, 15692 (2005).
- ¹²V. Kumar and T. P. Sharma, *Opt. Mater.* **10**, 253 (1998).
- ¹³H. Wei, X. L. Ren, Z. Y. Han, T. T. Li, Y. J. Su, L. M. Wei, F. S. Cong, and Y. F. Zhang, *Mater. Lett.* **102**, 94 (2013).
- ¹⁴M. A. Mahdi, J. J. Hassan, Z. Hassan, and S. S. Ng, *J. Alloys Compd.* **541**, 227 (2012).
- ¹⁵T. Y. Zhai, X. S. Fang, H. B. Zeng, X. J. Xu, Y. S. Bando, and D. Golberg, *Pure Appl. Chem.* **82**, 2027 (2010).
- ¹⁶W. Yu, P. F. Fang, and S. J. Wang, *J. Alloys Compd.* **486**, 780 (2009).
- ¹⁷C. Q. Jin, W. Zhong, X. Zhang, Y. Deng, C. Au, and Y. W. Du, *Cryst. Growth Des.* **9**, 4602 (2009).
- ¹⁸Y. Y. Xi, T. L. Y. Cheung, and D. H. L. Ng, *Mater. Lett.* **62**, 128 (2008).
- ¹⁹T. Y. Zhai, Z. J. Gu, W. S. Yang, X. Z. Zhang, J. Huang, Y. S. Zhao, D. P. Yu, H. B. Fu, Y. Ma, and J. N. Yao, *Nanotechnology* **17**, 4644 (2006).
- ²⁰J. J. Cai, J. S. Jie, P. Jiang, D. Wu, C. Xie, C. Y. Wu, Z. Wang, Y. Q. Yu, L. Wang, X. W. Zhang, Q. Peng, and Y. Jiang, *Phys. Chem. Chem. Phys.* **13**, 14663 (2011).
- ²¹G. Perna, S. Pagliara, V. Capozzi, M. Ambrico, and M. Pallard, *Solid State Commun.* **114**, 161 (2000).
- ²²P. Cherlin, E. L. Lind, and E. A. Davis, *J. Electrochem. Soc.* **117**, 233 (1970).
- ²³M. Feng, L. B. Luo, B. Nie, and S. H. Yu, *Adv. Funct. Mater.* **23**, 5116 (2013).
- ²⁴D. Gedamu, I. Paulowicz, S. Kaps, O. Lupan, S. Wille, G. Haidarschin, Y. K. Mishra, and R. Adelung, "Rapid Fabrication Technique for Interpenetrated ZnO Nanotetrapod Networks for Fast UV Sensors," *Adv. Mater.* (published online).
- ²⁵Z. B. He, J. S. Jie, W. J. Zhang, W. F. Zhang, L. B. Luo, X. Fan, G. D. Yuan, I. Bello, and S. T. Lee, *Small* **5**, 345 (2009).
- ²⁶J. S. Jie, W. J. Zhang, Y. Jiang, X. M. Meng, Y. Q. Li, and S. T. Lee, *Nano Lett.* **6**, 1887 (2006).
- ²⁷L. B. Luo, F. X. Liang, and J. S. Jie, *Nanotechnology* **22**, 485701 (2011).